Combining topology optimization with ecodesign for optimal fiber placement of thin structures

Joseph Morlier, Frederic Lachaud, Gustavo Asai

CSMA 2024
16ème Colloque National en Calcul des Structures
13-17 Mai 2024, Presqu'île de Giens (Var)

Combining topology optimization with ecodesign for optimal fiber placement of thin structures

G. Asai[1,2], F. Lachaud[3], J. Morlier[3]

[1] *ISAE-SUPAERO, Université de Toulouse, DMSM, France, gustavo.asai@student.isae-supaero.fr*
[2] *Instituto Tecnológico de Aeronáutica (ITA), Brazil, asai@ita.br*
[3] *ICA, Université de Toulouse, ISAE-SUPAERO, MINES ALBI, UPS, INSA, CNRS, Toulouse, France, {frederic.lachaud,joseph.morlier}@isae-supaero.fr*

Résumé — This work aims at studying new topology optimization methods for 3D printed eco-optimized structures. The first step consists in the validation of the extension of bidimensional optimization of topology and fiber orientations so that it can be used in three dimensions. The complete optimization was then performed considering both mechanical performance and environmental impact, showing the potential advantages of natural fibers in aerostructures.
Mots clés — topology optimization, ecodesign, natural fibers.

1 Introduction

The accelerated development of 3D printing technology has allowed the evolution of the existing methods for structural design, making viable the extensive use of topology optimization, for example. Composite materials are also becoming of great importance in the aerospace industry, and materials of natural origin are as well subject of this study, with the goal of building efficient eco-optimized structures.

For isotropic optimizations, the material choice can be decoupled from the topology optimization [1, 2]. However, the mechanical properties of anisotropic materials influence the final geometry obtained, so that the optimization has to be done simultaneously to the material choice. The objective of this work is to study the use of topology optimization to design 3D printable thin structures while taking into account the environmental impact along with the mechanical performance.

2 Literature Review

2.1 Solid Isotropic Material with Penalization (SIMP)

Solid Isotropic Material with Penalization (SIMP) is a finite element-based method for topology optimization. For each element, a density value ρ_e within the range from 0 (void element) to 1 (filled element) is assigned. To enforce the convergence to a predominantly 0/1 configuration (the only physically feasible values, there is no intermediate material), the material properties for each element are obtained from a power-law interpolation, i.e. dependent on ρ_e^p, where p is a penalization factor (typically $p = 3$).

A topology optimization problem where the objective is to minimize the compliance c can be written as (1) [3], where $\boldsymbol{U}$ and $\boldsymbol{F}$ are the global displacement and force vectors, respectively, $\boldsymbol{K}$ is the global stiffness matrix, $\boldsymbol{u_e}$ and $\boldsymbol{k_e} = \rho_e^p \boldsymbol{k_0}$ are the element displacement vector and stiffness matrix, respectively, $\boldsymbol{\rho}$ is the vector of design variables, ρ_{min} is the minimum relative density (non-zero to avoid singularity), $V(\boldsymbol{\rho})$ and V_0 are the material volume and design domain volume, and f is the prescribed volume fraction.

$$\begin{aligned} &\min_{\boldsymbol{\rho}} c(\boldsymbol{\rho}) = \boldsymbol{U}^{\boldsymbol{T}} \boldsymbol{K} \boldsymbol{U} = \sum_e \rho_e^p \, \boldsymbol{u_e^T} \, \boldsymbol{k_0} \, \boldsymbol{u_e} \\ &\text{subject to} \begin{cases} \frac{V(\boldsymbol{\rho})}{V_0} \leq f \\ \boldsymbol{K} \boldsymbol{U} = \boldsymbol{F} \\ 0 < \rho_{min} \leq \boldsymbol{\rho} \leq 1 \end{cases} \end{aligned} \tag{1}$$

To avoid the appearance of checkerboard patterns and to ensure the mesh-independence of the result, the element sensitivities are filtered by a linear decaying convolution filter (2), where r_ρ is a fixed filter

radius and $\Delta(e,i)$ is the distance operator between the centers of elements e and i.

$$\widetilde{\rho_e \frac{\partial c}{\partial \rho_e}} = \frac{1}{\sum_i H_{ei}^{\rho}} \sum_i H_{ei}^{\rho} \rho_i \frac{\partial c}{\partial \rho_i}, \quad H_{ei}^{\rho} = \max(0, r_{\rho} - \Delta(e,i)) \tag{2}$$

2.2 Continuous Fiber Angle Optimization (CFAO)

For a given domain, the determination of fiber orientations can be performed using various approaches. A method that emerged is the Discrete Material Optimization (DMO), in which the orientations are chosen from a predefined finite set of possibilities, defining different materials that can be used. It is useful for composite laminates for example, but it is not suitable for 3D printing as it does not ensure fiber continuity. On the other side of the spectrum, Free Material Optimization (FMO) treats the stiffness tensor components as design variables, increasing the freedom in the design, although sometimes leading to infeasible material properties.

In Continuous Fiber Angle Optimization (CFAO), an orientation is assigned for each element, a methodology that is appropriate in the in the context of the Fused Filament Fabrication (FFF) [4, 5] and that can be easily integrated to the SIMP method, adjusted to yield continuous orientations over the domain. However, this approach may present local minima due to the periodicity of the angle, that can be avoided by using the correct representation of the orientations with the design variables.

2.3 SIMP extended with CFAO

The SIMP method can then be extended with CFAO as (3), creating a modified 2D problem where both sets of variables are simultaneously optimized [6]. As a non-convexity may arise from the periodicity of the angle variable, another possible approach is to define the orientation using the Cartesian components of the orientation vector [7].

$$\begin{aligned} &\min_{\boldsymbol{\rho},\boldsymbol{\theta}} c(\boldsymbol{\rho},\boldsymbol{\theta}) = \sum_e \rho_e^p \, \boldsymbol{u_e^T} \, \boldsymbol{k_0}(\theta_e) \, \boldsymbol{u_e} \\ &\text{subject to} \begin{cases} \frac{V(\boldsymbol{\rho})}{V_0} \leq f \\ \boldsymbol{KU} = \boldsymbol{F} \\ 0 < \rho_{min} \leq \boldsymbol{\rho} \leq 1 \\ -\frac{\pi}{2} \leq \boldsymbol{\theta} \leq \frac{\pi}{2} \end{cases} \end{aligned} \tag{3}$$

In both formulations, a filter is necessary to regularize the orientations and create a smoothly varying field that can be more easily converted to a printable structure. There is a wider range of choices for this filter, which is independent of the filter applied to the densities. Within each iteration, it can be applied on the sensitivities [8], on the material tensor [9], on the angles [10], or on the angles Cartesian projections [11]. Furthermore, the type of filter can also vary, such as using a Gaussian filter instead of the convolution filter with weights decaying linearly [8]. Even though the method is fairly consolidated for 2D optimizations, there are multiple possibilities to extend the problem to 3D, with varying levels of computational cost, manufacturing easiness, and design space freedom :

— Choose a printing direction and divide the domain in layers [6]
— Define allowable printing planes to make components that can be later assembled [11]
— Optimise geometric primitives (plates, bars) as discrete components [12, 13]
— Introduce design variables to define free 3D fiber orientations by spherical coordinates [10]

Additionally, the formulation can be easily adapted to solve different problems, such as mass minimization or optimization with stress constraints [14].

3 Numerical framework

3.1 Implementation

The algorithm was implemented in Python, using the Method of Moving Asymptotes (MMA) [15] as variable updating scheme and Ansys as finite element solver. The latter allows a straightforward mesh and boundary conditions creation, which can be time-consuming to perform by hand for complex geometries.

The global stiffness matrix assemblage step is then abstracted, but the algorithm is still dependent on the construction of elemental stiffness matrices $\boldsymbol{k_0}$ to calculate sensitivities. For 2D optimizations, the implementation assumes a 4-node quadrilateral element (Ansys element type PLANE182) and for 3D optimizations, an 8-node brick element (SOLID185).

The problem formulation is the same as (3), with the assumption of 2D or 3D optimization lying on the definition of $\boldsymbol{k_0}$. This corresponds to choosing the z axis as printing direction, with fibers oriented inside the plane xy. Densities were filtered using the convolution filter (2) and a similar convolution filter (4) was applied at each iteration for orientation smoothing, adjusted to reduce the weight of void elements, where the desired minimum fiber curvature, controlled by r_θ, is independent from r_ρ.

$$\tilde{\theta}_e = \frac{1}{\sum_i H^\theta_{ei}\rho_i}\sum_i H^\theta_{ei}\rho_i\theta_i, \quad H^\theta_{ei} = \max(0, r_\theta - \Delta(e,i)) \tag{4}$$

Due to the non-convexity of this optimization problem and the presence of many local minima, the results are strongly dependent on the initial orientations. One possible workaround is to choose random initial orientations for each element, which should be a good approximation for the global minimum when the optimal initial orientation is not known [10]. Additionally, the continuation method in [16] was applied on the penalization factor p. Instead of having a fixed value throughout the whole optimization, it starts at $p = 1$ and is increased each time a convergence in compliance is achieved. The stopping criterion for the continuation is the greyness level of the design, i.e., when the proportion of elements that are neither void nor filled is below a certain level.

3.2 Material modeling

The materials were modeled as transverse isotropic, suitable for matrices reinforced by unidirectional fibers. The fibers were considered to be aligned with the local x axis, which can be characterised by five independent elastic constants : longitudinal and transverse Young's moduli, in-plane and out-of-plane Poisson's ratios, and in-plane shear modulus, which were calculated from fiber and resin properties using the rule of mixtures. The final material orientation within an element is obtained by a rotation θ_e around the z axis, represented by the rotation matrix $\boldsymbol{T_\theta}$ in (5).

$$\boldsymbol{T_\theta}(\theta_e) = \begin{bmatrix} c_\theta^2 & s_\theta^2 & 0 & 0 & 0 & -2s_\theta c_\theta \\ s_\theta^2 & c_\theta^2 & 0 & 0 & 0 & 2s_\theta c_\theta \\ 0 & 0 & 1 & 0 & 0 & 0 \\ 0 & 0 & 0 & c_\theta & s_\theta & 0 \\ 0 & 0 & 0 & -s_\theta & c_\theta & 0 \\ c_\theta s_\theta & -c_\theta s_\theta & 0 & 0 & 0 & c_\theta^2 - s_\theta^2 \end{bmatrix}, \; c_\theta = \cos\theta_e, \; s_\theta = \sin\theta_e \tag{5}$$

3.3 Sensitivity analysis

As the MMA is gradient-based, it is necessary to calculate sensitivities of the objective function with respect to the design variables in (6). The value of $\boldsymbol{k_0}$ is not explicitly calculated, since $\frac{\partial c}{\partial \rho_e}$ can be obtained from the elemental strain energy $\rho_e^p \boldsymbol{u_e^T k_0}(\theta_e)\boldsymbol{u_e}$ gathered from Ansys results. However, $\frac{\partial \boldsymbol{k_0}}{\partial \theta_e}$ is not directly accessible in Ansys and has to be integrated from the element strain-displacement matrix $\boldsymbol{B_e}$ and the material constitutive matrix $\boldsymbol{C}$ using (7). The integrals were evaluated with 2-point Gaussian quadrature, which is exact for the chosen element formulations (linear in each natural coordinate).

$$\frac{\partial c}{\partial \rho_e} = -p\rho_e^{p-1}\boldsymbol{u_e^T k_0 u_e}, \quad \frac{\partial c}{\partial \theta_e} = -\rho_e^p \boldsymbol{u_e^T}\frac{\partial \boldsymbol{k_0}}{\partial \theta_e}\boldsymbol{u_e} \tag{6}$$

$$\frac{\partial \boldsymbol{k_0}}{\partial \theta_e}(\theta_e) = \iiint \boldsymbol{B_e^T}\left(\frac{\partial \boldsymbol{T_\theta}}{\partial \theta_e}\boldsymbol{C}\boldsymbol{T_\theta^T} + \boldsymbol{T_\theta}\boldsymbol{C}\frac{\partial \boldsymbol{T_\theta^T}}{\partial \theta_e}\right)\boldsymbol{B_e}\, d\boldsymbol{\Omega} \tag{7}$$

3.4 CO_2 footprint assessment

In this work, the environmental impact of the structure is measured in terms of the mass of CO_2 emitted during material production $CO_{2,mat}$ and during its use in a long distance aircraft $CO_{2,use}$, following

the methodology from [1], adapted to composite materials. The value used to compare different designs is the total footprint $CO_{2,tot} = CO_{2,mat} + CO_{2,use}$.

The impact of the material production depends on the total mass M and the CO_2 intensity of the material $CO^i_{2,mat}$ (mass of CO_2 emitted per mass of material). Its expression is given by (8), where ρ_f is the fiber density, $CO^i_{2,f}$ is the fiber CO_2 intensity, ρ_m is the matrix density, $CO^i_{2,m}$ is the matrix CO_2 intensity, and V_f is the fiber volume fraction in the composite material.

$$CO_{2,mat} = M \cdot CO^i_{2,mat} = M \cdot \frac{\rho_f V_f CO^i_{2,f} + \rho_m (1 - V_f) CO^i_{2,m}}{\rho_f V_f + \rho_m (1 - V_f)} \tag{8}$$

The impact of the use phase is calculated as the emissions that would be saved if the component was lighter. Reducing the mass by 1 kg in a long distance aircraft leads to a reduction of 98.8 tCO_2 during its lifetime [1], i.e., $CO_{2,use} = M \cdot 98.8\ \text{t}CO_2/\text{kg}$.

4 Results and discussion

The reference problem is a half Messerschmitt–Bölkow–Blohm (MBB) beam, with boundary conditions shown in Fig. 1. The optimization was performed in a 168 mm × 80 mm × 8 mm half beam, divided in elements with side length equal to 4 mm and subject to a vertical force $F = 1$ kN.

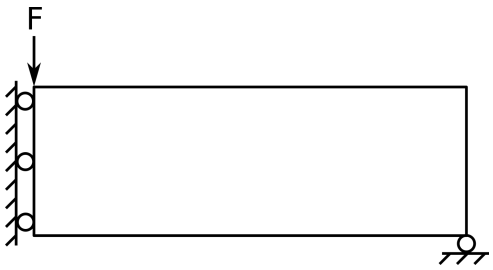

FIGURE 1 – Half MBB beam problem.

4.1 Use of 3D elements

The first numerical experiment aims to validate the extension of the problem formulation from two to three dimensions, by verifying the equivalence between the results using 2D and 3D elements. For both meshes, the problem was solved for $f = 0.3$, $r_\rho = 8$ mm, $r_\theta = 20$ mm, and initial orientation of $-30°$. As the filter radii are greater than the domain thickness, all layers (in z direction) of the 3D design are forced to be similar, which should result in a final geometry equivalent to the 2D case. The material used is cellulose reinforced with 0.5 volume fraction of bamboo fiber, $E_x = 10.37$ GPa, $E_y = 5.48$ GPa, $\nu_{xy} = 0.1975$, and $G_{xy} = 2.1$ GPa.

For this analysis, p was set to 3 (without continuation) and the algorithm was run for 100 iterations, shown in Figure 2. The 2D model reached a compliance of 2736 N.mm, while the 3D reached 2760 N.mm, with a relative difference of 0.9%. Final topologies and fiber configurations are qualitatively almost identical and the compliance histories are similar during the optimization, indicating the good agreement between both formulations.

By using 3D elements, it is possible to capture the out-of-plane Poisson effect, leading to slightly different orientations only in the constrained regions. When the filters allow more independence between the layers, the 3D optimization provides more freedom on the spatial material distribution, potentially resulting in more efficient structures. The main drawback is the higher computation time due to the increased number of design variables and degrees of freedom in the finite element model. In this example, the total optimization times were 717 seconds (for 2D) and 1040 seconds (for 3D), representing a 45.0% increase.

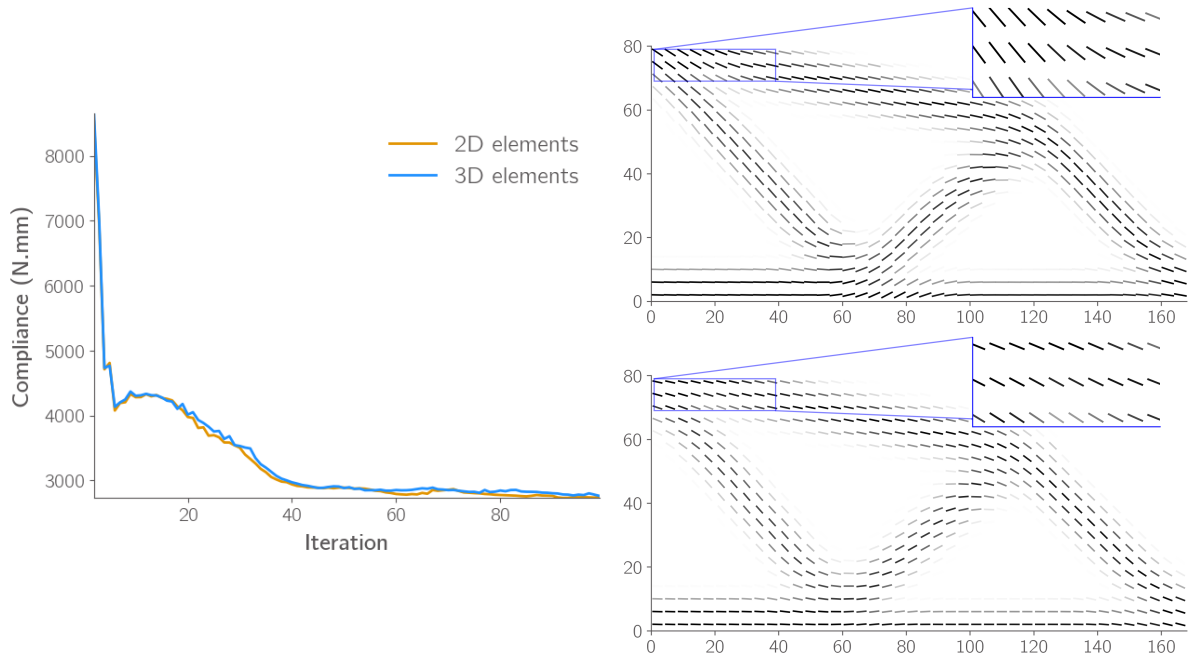

FIGURE 2 – Compliance history and final designs : 2D optimization (top) and bottom layer of the 3D optimization (bottom). The main difference is in the orientations near the force application point.

4.2 Material optimization

A material optimization was performed on the same MBB beam, using 3D elements with side length of 4 mm. For all run cases, the filter parameters were set as $r_\rho = 8$ mm and $r_\theta = 20$ mm. Initial angles were randomly chosen for each element and the continuation method on the penalization was applied. All possible combinations of fibers and resins in Table 1, with fiber volume fraction of 0.5, were optimised for $f = 0.3$.

TABLE 1 – Properties of available materials.

Material		ρ (kg/m^3)	E (GPa)	ν	CO_2^i (kg CO_2/kg)
Fibers	Bamboo	700	17.5	0.04	1.0565
	Flax	1470	53.5	0.355	0.44
	Hemp	1490	62.5	0.275	1.6
	Carbon High Modulus	2105	760	0.105	68.1
	Carbon Low Modulus	1820	242.5	0.105	20.3
	S-Glass	2495	89.5	0.22	2.905
	E-Glass	2575	78.5	0.22	2.45
Resins	Cellulose	990	3.25	0.355	3.8
	PLA	1290	5.19	0.39	2.115
	PETG (abs)	1270	2.06	0.403	4.375
	Epoxy	1255	2.41	0.399	5.94
	Polyester	1385	4.55	0.35	4.5

Figure 3 shows the compliance and CO_2 footprint for each material configuration. For this aeronautical use case, the values of $CO_{2,use}$ are orders of magnitude greater than $CO_{2,mat}$, in such a way that minimizing the footprint is essentially equivalent to minimizing the mass. Natural fibers are then great options because of their lower densities, with flax and hemp structures reaching compliance values similar to glass but with lower CO_2 emission and mass. Regarding the resins, cellulose stands out for reducing the CO_2 footprint with little to no compliance cost.

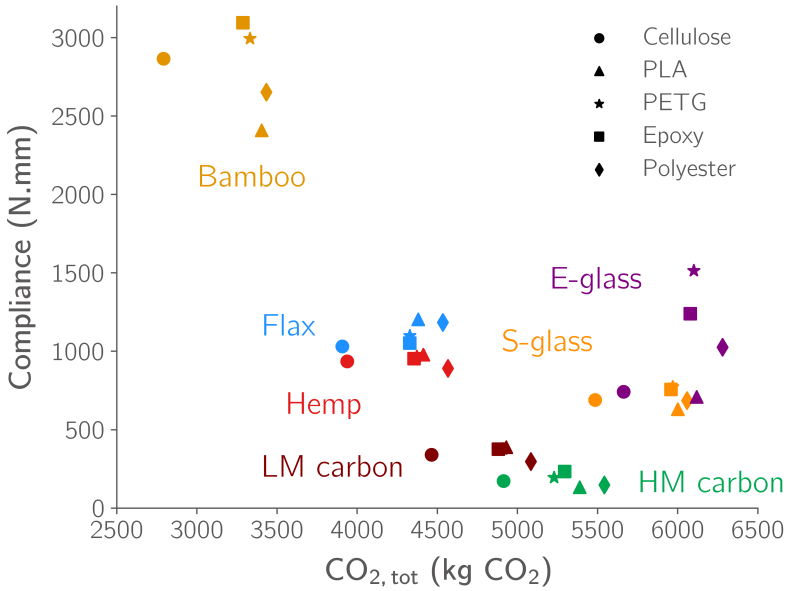

FIGURE 3 – Compliance versus CO_2 footprint of the optimal designs. Each point represents a fiber/resin optimization, colored by fiber.

4.3 Structural versus non structural parts in aeronautics

To verify the gains in mass and CO_2 footprint that the natural fibers can provide, they were compared to standard composites in two use cases, structural and nonstructural components. For main structural components, where stiffness is an important requirement, carbon fiber is typically used. A HM carbon/epoxy and a hemp/cellulose design (with 0.5 fiber volume fraction) were optimized to achieve a compliance of 500 N.mm by varying f. For the aeronautical domain, given that the environmental impact is strongly dependent on the mass, Table 2 shows that the increase in material required to compensate the reduction in stiffness leads to a 170.9% greater footprint when using hemp fibers compared to the carbon fibers. However, in a static use case where the material production has the most impact, the hemp fiber structure could give the same compliance with 93.8% less CO_2 emission.

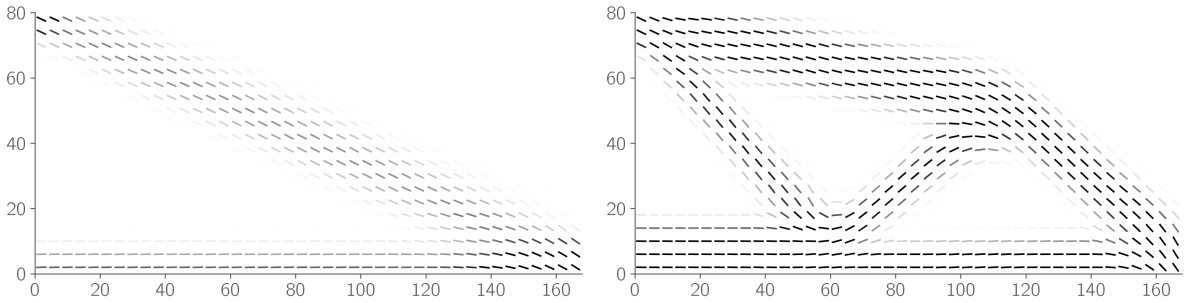

FIGURE 4 – Final designs with target compliance of 500 N.mm : HM carbon/epoxy (left) and hemp/cellulose (right).

TABLE 2 – Structures optimised for a target compliance of 500 N.mm.

Fiber	Resin	f	Compliance (N.mm)	M (g)	$CO_{2,tot}$ (kg CO_2)	$CO_{2,mat}$ (kg CO_2)
HM Carbon	Epoxy	0.116	503	20.9	2060	2.25
Hemp	Cellulose	0.425	503	56.6	5581	0.14

For non structural parts, where providing stiffness is not the main function, e.g. aircraft interior, fiber-

glass is a typical choice. A bamboo/cellulose design was considered as substitute to minimize footprint for fixed f. Results for $f = 0.3$ are shown in Fig. 5 and Table 3, bamboo presents a reduction in mass and CO_2 emission by a factor of 2.4 but with 3.7 times more compliance, which might be acceptable when loading is not critical.

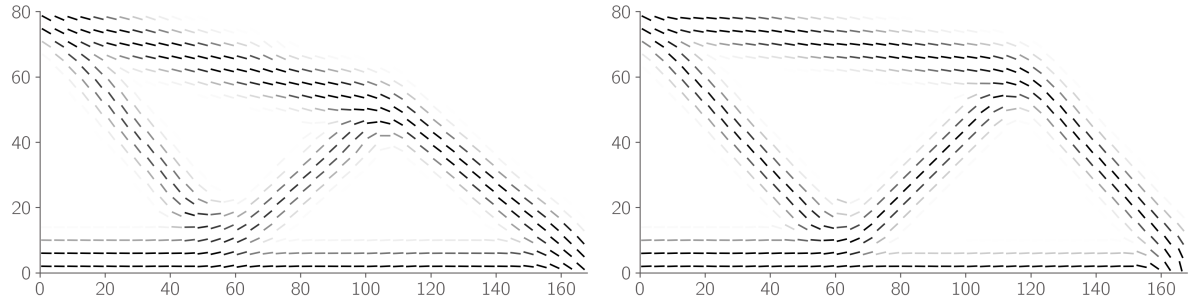

FIGURE 5 – Final designs optimised at $f = 0.3$: S-glass/polyester (left) and bamboo/cellulose (right).

TABLE 3 – Structures optimised for minimum footprint at $f = 0.3$.

Fiber	Resin	Compliance (N.mm)	M (g)	$CO_{2,tot}$ (kg CO_2)
S-glass	Polyester	574	65.2	6160
Bamboo	Cellulose	2136	27.2	2682

5 Conclusions

The 3D CFAO code is still in progress. It has been validated on 2D thin structures. The code to reproduce the analysis and optimizations is available at `https://github.com/mid2SUPAERO/SOMP_Ansys/tree/csma`.

When optimising for mass and CO_2 footprint, bio-sourced materials present preliminary advantages against traditional aeronautical composites, especially for non structural components, where bamboo/cellulose can replace fiberglass. For structural components, the substitution from carbon fiber to hemp fiber involves finding a compromise between compliance and environmental impact. A next step is printing the obtained structures to experimentally verify the results.

6 Acknowledgements

The authors acknowledge the support from Alexandre Coelho and Kunal Masania on the project development. This study was financed in part by the Coordenação de Aperfeiçoamento de Pessoal de Nível Superior - Brasil (CAPES) - Finance Code 001.

Références

[1] E. Duriez, J. Morlier, C. Azzaro-Pantel, M. Charlotte. *Ecodesign with topology optimization*, Procedia CIRP, Elsevier, 454-459, 2022.

[2] E. Duriez, C. Azzaro-Pantel, J. Morlier, M. Charlotte. *A fast method of material, design and process eco-selection via topology optimization, for additive manufactured structures*, Cleaner Environmental Systems, Elsevier, 100114, 2023.

[3] O. Sigmund. *A 99 line topology optimization code written in Matlab*, Structural and multidisciplinary optimization, Springer, 120-127, 2001.

[4] D. Jiang. *Three dimensional topology optimization with orthotropic material orientation design for additive manufacturing structures*, Master's thesis, Baylor University, 2017.

[5] R.M. Hoglund. *An anisotropic topology optimization method for carbon fiber-reinforced Fused Filament Fabrication*, Master's thesis, Baylor University, 2016.

[6] D. Jiang, R. Hoglund, D.E. Smith. *Continuous fiber angle topology optimization for polymer composite deposition additive manufacturing applications*, Fibers, MDPI, 14, 2019.

[7] T. Nomura et al. *General topology optimization method with continuous and discrete orientation design using isoparametric projection*, International Journal for Numerical Methods in Engineering, Wiley Online Library, 571-605, 2015.

[8] E. Stragiotti. *Continuous Fiber Path Planning Algorithm for 3D Printed Optimal Mechanical Properties*, Master's thesis, Politecnico di Torino, 2020.

[9] D.R. Jantos, K. Hackl, P. Junker. *Topology optimization with anisotropic materials, including a filter to smooth fiber pathways*, Structural and Multidisciplinary Optimization, Springer, 2135-2154, 2020.

[10] M. Schmidt, L. Couret, C. Gout, C. Pedersen. *Structural topology optimization with smoothly varying fiber orientations*, Structural and Multidisciplinary Optimization, Springer, 3105-3126, 2020.

[11] Z. Qiu, Q. Li, Y. Luo., S. Liu. *Concurrent topology and fiber orientation optimization method for fiber-reinforced composites based on composite additive manufacturing*, Computer Methods in Applied Mechanics and Engineering, Elsevier, 114962, 2022.

[12] H. Smith, J. Norato. *Topology optimization with discrete geometric components made of composite materials*, Computer Methods in Applied Mechanics and Engineering, Elsevier, 113582, 2021.

[13] J. Greifenstein, E. Letournel, M. Stingl, F. Wein. *Efficient spline design via feature-mapping for continuous fiber-reinforced structures*, Structural and Multidisciplinary Optimization, Springer, 99, 2023.

[14] A. E. Moter. *Topology and Printing Orientation Optimization of Orthotropic Material for Additive Manufacturing*, Master's thesis, York University, 2021.

[15] K. Svanberg. *The method of moving asymptotes—a new method for structural optimization*, International journal for numerical methods in engineering, Wiley Online Library, 359-373, 1987.

[16] A. Castro Almeida, E. Duriez, F. Lachaud, J. Morlier. *New topology optimization for low CO_2 footprint AFP composite structures*, Poster session, WCSMO 2023.